Strain Field Self-Diagnostic Poly(dimethylsiloxane) Elastomers

CHEMISTRY OF MATERIALS

Article

pubs.acs.org/cm

# Strain Field Self-Diagnostic Poly(dimethylsiloxane) Elastomers

Andreas E. Früh,[†] Federico Artoni,[‡] Roberto Brighenti,*[,‡] and Enrico Dalcanale*[,†]

[†]Department of Chemistry, Life science and Environmental Sustainability, University of Parma and INSTM UdR Parma, Parco Area delle Scienze 17/A, 43124 Parma, Italy

[‡]Department of Engineering & Architecture, University of Parma, Parco Area delle Scienze 181/A, 43100 Parma, Italy

Supporting Information

**ABSTRACT:** Advanced applications, involving high risk mechanical systems, require the in-service deformation level to be verified in order to assess their safety and reliability, providing information for repairing or replacing interventions. In the present work, a self-diagnostic poly(dimethylsiloxane) (PDMS) elastomer containing a supramolecular detection probe is proposed, enabling the strain intensity in the polymeric matrix to be identified by fluorescence detection. Turn-on fluorescence represents an efficient, sensitive, simple, and real time diagnostic tool to quantitatively detect high-strain regions for the mechanical monitoring of structural elements. The supramolecular complex—cross-linking the polymer's chains—provides fluorescence response induced by strain even if present in a very low amount ($10^{-6}$ mol $kg^{-1}$), completely preserving the mechanical characteristics of the matrix. The developed PDMS material is mechanically tested, and the observed fluorescence field is correlated with that obtained by numerical simulations as well as by contactless measurements performed via the digital image correlation (DIC) technique.

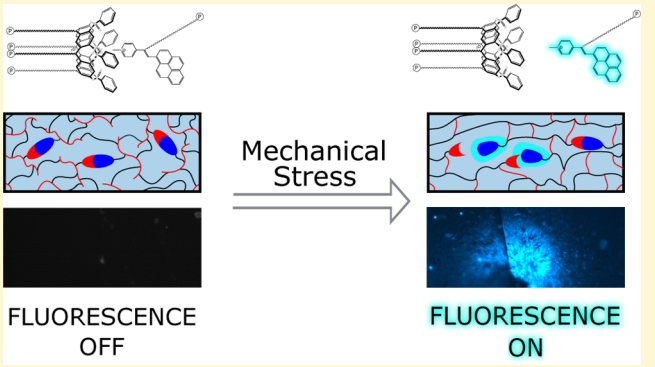


## INTRODUCTION

Polymers are desirable materials for high-performance applications, due to their affordable price, light weight, and processability. However, small damages, which are difficult to detect, can compromise the mechanical integrity of the material and subsequently lead to failure. Molecular probes are ideal candidates to facilitate the detection of such damages and thus to prevent catastrophic failure, visualizing mechanical strain and/or damage as an easily detectable alert signal at a very early stage. A range of mechanochemical reporters, based on force induced redistributions of a chemical equilibrium, have been published,[1−6] including spiropyran-[7−10] and dioxetane-[11−14] based systems. Other systems are based on physical effects such as aggregation or separation-induced emission,[15,16] alteration of the band gap by physical deformation of SWCNT,[17,18] or mechanochromism.[19−21] However, those probes have the drawback that relatively large quantities of the active system are needed, which alters the mechanical properties of the polymer and significantly increases the price of the material. Probes based on the force induced redistributions of a chemical equilibrium add covalent cross-links to the system. Systems based on physical effects, like the aggregation or separation-induced emission, are relatively sensitive, but they need specially engineered polymers, in the form of solvent-filled microcapsules or the layering of different materials. PDMS elastomers are among the polymeric matrices used to detect mechanical damage with mechanophores.[22] In a step forward, Sijbesma et al. reported a strain-field sensitive mechanoluminescent PDMS elastomer equipped with dioxetane cross-linkers, capable of reporting "mechanomemory" effects in the polymer.[23]

In hydrostatic stress-sensitive materials containing microvoids or microdefects, the knowledge of the volumetric strain is fundamental for their safety level assessment yet demanding to determine in service.[24,25] The volumetric strain physically corresponds to the mean strain value, obtained by averaging the strain components with respect to all the 3D space directions.[26] In such materials, the presence of a tensile hydrostatic stress state can lead to an expansion and coalescence of microvoids and inclusions (often identified as cavitation-like failure), triggering the subsequent crack appearance and growth.[27]

The above-described mechanism becomes much more relevant in the case of materials withstanding repeated loads (fatigue). The capability to monitor the maximum volumetric strain occurring in the element under service enables its design to be optimized and the safety level to be enhanced. The direct measure of the average strain is not feasible, and the determination of the volumetric strain requires strain measurements in multiple directions, an operation that can be prohibitive in small or thin elements. A possible solution is adding a probe capable of detecting and reporting mechanical deformations at the molecular level. The availability of a

Received: June 12, 2017
Revised: July 31, 2017
Published: July 31, 2017





DOI: 10.1021/acs.chemmater.7b02438
Chem. Mater. XXXX, XXX, XXX−XXX

molecular-based detection tool is highly desirable to map highly volumetric strained regions without the need of any complex measurement device and without affecting the microstructure bearing capability of the material. Further, self-diagnostic capability allowed by molecular interactions (i.e., at the nanoscale level) entails no restrictions on the scale of the element to be analyzed and opens the way to the monitoring of objects of any size.

In this paper, we introduce a self-diagnostic PDMS elastomer containing a supramolecular detection probe, which is able to report areas of high strain in the polymeric matrix by fluorescence turn-on. Turn-on fluorescence, which is easily detectable with suitable equipment, offers an excellent contrast between high-strain affected and unaffected regions, providing a very sensitive tool for the monitoring of structural elements.

## EXPERIMENTAL SECTION

**Synthesis.** *4-(Dodec-11-en-1-yl)pyridine.* 4-Picoline (2.6 mL, 29.17 mmol) was dissolved in dry THF (12 mL), and the solution was cooled to −41 °C with an acetonitrile−liquid nitrogen slush bath.[28] *n*-Butyllithium in hexanes (2.5 M, 13.5 mL, 33.75 mmol) was added over 30 min. The reaction was stirred for an additional 5 min at −41 °C, and then the bath was removed and the reaction allowed to warm up to room temperature. After 1 h, additional dry THF (12 mL) was added to dilute the 4-picolyllithium slurry and the obtained solution stirred for 1 h more. The solution was cooled with an ice bath to 0 °C and added over 30 min into a solution of 11-bromo-1-undecene (7.0 mL, 31.91 mmol) in THF (5.0 mL) at −41 °C. The reaction was allowed to warm up to room temperature and stirred for 21 h. Water (1.5 mL) was added, the obtained mixture filtered over a silica pad, and the pad washed with ethyl acetate (6 × 30 mL). The organic phases were combined, the solvent removed, and the residue further purified by flash chromatography (Hex/EtOAc 1.5/1), yielding a yellow oil (4.15 g, 50% yield). $^1$H NMR (300 MHz, $CDCl_3$) $\delta$: 8.42 (d, $J$ = 6.0 Hz, 2H, $\alpha$ Py H), 7.03 (d, $J$ = 5.5 Hz, 2H, $\beta$ Py H), 5.75 (ddt, $J$ = 17.0, 10.3, 6.7 Hz, 1H, C$\underline{H}$=$CH_2$), 4.97−4.85 (m, 2H, CH=C$\underline{H_2}$), 2.53 (t, $J$ = 7.7 Hz, 2H, Py−C$\underline{H_2}$), 1.98 (q, $J$ = 7.0 Hz, 2H, C$\underline{H_2}$−CH=$CH_2$), 1.55 (q, $J$ = 7.3 Hz, 2H, Py−$CH_2$−C$\underline{H_2}$), 1.34−1.22 (m, 15H). $^{13}$C NMR (75 MHz, $CDCl_3$, $\delta$): 151.5 ($\gamma$ Ar C), 149.5 ($\alpha$ Py C), 139.0 (C$\underline{H}$=$CH_2$), 123.8 ($\beta$ Py C), 114.1 (CH=C$\underline{H_2}$), 35.2 (Py−C$\underline{H_2}$), 33.7 (C$\underline{H_2}$−CH=$CH_2$), 30.2, 29.50, 29.44, 29.42, 29.34, 29.12, 29.07, 28.87. MS (ESI) $m/z$: $[M + H]^+$ calcd for $C_{17}H_{28}N$, 246.22; found, 246.28.

*N-Methyl-4-(dodec-11-en-1-yl)pyridinium Iodide.* 4-(Dodec-11-en-1-yl)pyridine (561 mg, 2.29 mmol) was dissolved in iodomethane (4.0 mL, 46.3 mmol) and refluxed under nitrogen for 6 h. The product was precipitated with diethyl ether, filtered off, washed with diethyl ether, and dried in vacuo, yielding an off-white solid (884 mg, 100%). $^1$H NMR (300 MHz, $CDCl_3$) $\delta$: 9.24 (d, $J$ = 6.6 Hz, 2H, $\alpha$ Py H), 7.84−7.80 (m, 2H, $\beta$ Py H), 5.87−5.71 (m, 1H, C$\underline{H}$=$CH_2$), 5.01−4.84 (m, 2H, CH=C$\underline{H_2}$), 4.63 (s, 3H, N-C$\underline{H_3}$), 2.90−2.81 (m, 2H, Py-C$\underline{H_2}$), 2.06−1.94 (m, 2H, C$\underline{H_2}$-CH=$CH_2$), 1.74−1.60 (m, 2H, Py-$CH_2$−C$\underline{H_2}$), 1.32−1.18 (m, 15H). MS (ESI) $m/z$: $[M - \text{Iodine}]^+$ calcd for $C_{18}H_{30}N$, 260.24; found, 260.27.

*N-Methyl-4-(1-(pyren-1-yl)trideca-1,12-dien-2-yl) Pyridinium Iodide (Guest).* 1-Pyrenecarboxaldehyde (400 mg, 1.74 mmol) was dissolved in ethanol (3.0 mL), and *N*-methyl-4-(dodec-11-en-1-yl)pyridinium iodide (236 mg, 0.61 mmol) and piperidine (200 $\mu$L) were added. The reaction was stirred under reflux for 16 h, then the solvent removed, and the obtained crude purified by flash chromatography (DCM/MeOH 95/5), yielding an orange solid (44 mg, 12%). $^1$H NMR (300 MHz, $CDCl_3$) $\delta$: 9.27 (d, $J$ = 6.7 Hz, 2H, $\alpha$ Py H), 8.82 (d, $J$ = 6.7 Hz, 2H, $\beta$ Py H), 8.23−7.96 (m, 8H, Pyrene), 7.56 (d, 1H, H(10)−Pyrene), 5.83−5.72 (m, 1H, C$\underline{H}$=C), 5.05−4.90 (m, 1H,), 4.70 (s, 3H, N−C$\underline{H_3}$), 2.89−2.71 (m, 2H, Py−C$\underline{H}$), 2.06−1.94 (m, 2H, C$\underline{H_2}$−CH=$CH_2$), 1.64−1.60 (m, 2H, Py-$CH_2$−C$\underline{H_2}$), 1.44−1.04 (m, 15H). MS (ESI) $m/z$: $[M - I]^+$ calcd for $C_{35}H_{38}N$, 472.30; found, 472.34.

*Tetraphosphonate Cavitand Host.* The host was prepared following a published procedure.[29,30]

**PDMS Preparation.** A commercially available room temperature vulcanization silicone kit, RTV 615 (Momentive Performance Materials Inc., Waterford, NY) was used to prepare the matrix.

Dichloromethane solution of guest ($c = 10^{-5}$ M) and host ($c = 2 \times 10^{-5}$ M) were prepared in order to form the supramolecular complex and to easily measure the desired quantities. The required quantities of the solutions or a mixture thereof was added to component A of RTV 615 and the solvent subsequently removed by warming the component to 60 °C. Mixing of the preloaded component A with component B and subsequent curing at 40 °C overnight yielded the used polymer samples.

**Fluorescence Characterization.** Samples for fluorescence characterization were prepared using the required amount of guest solution with or without an equivolumar amount host solution in order to obtain samples with a concentration of $b$(guest) = $10^{-6}$ mol $kg^{-1}$. Preparation was performed as described above, and the obtained samples were cured at 40 °C overnight directly in cuvettes (poly(methyl methacrylate), path length 10 mm, Sigma-Aldrich Z188018). Spectra were recorded on a PerkinElmer LS 55 Fluorescence spectrometer using FL WinLab.[31] Data was plotted using gnuplot.[32]

**Stress Test Samples.** Samples for mechanical stress tests were prepared using the required amount of guest solution mixed with an equivolumar amount of host solution in order to obtain samples with a concentration of $b$(guest) = $10^{-6}$ mol $kg^{-1}$. Blank samples were prepared without any additions. Samples were cured in a custom-made aluminum mold, yielding specimens with the dimensions shown in Figure 8.

The obtained precracked samples were mechanically tested under a three-point bending system; a vertical controlled downward displacement $\delta$ was applied to the top central point of the beam at a rate equal to about $\delta = 5 \times 10^{-5}$ m $s^{-1}$; the corresponding restraint force $F$ (see Figure 8a) was measured during the test. The applied displacement $\delta$ was increased until the crack started growing upward (leading roughly to the development of a crack nearly along the middle cross-section of the beam specimen; see Figure 10) and continuously increased until the crack reached a final length equal to about 3 times its initial size before the final failure of the specimen. Besides mechanical and kinematic measurements, the specimens were also monitored through the Digital Image Correlation (DIC) technique to quantitatively measure the displacement and the strain field of the surface of the specimen.

High resolution pictures ware taken for some increments of the applied displacement at a step equal to $\Delta\delta = 5 \times 10^{-4}$ m and processed through the freely available DIC analyzer NCORR software.[33,34]

After the mechanical test, the samples were examined using a Nikon Eclipse Ti (Nikon Corp., Tokyo, Japan) equipped with a UV-1A ultraviolet excitation filter block (Nikon Corp., Tokyo, Japan; excitation filter wavelengths: 360−370 nm (bandpass, 365 CWL); dichromatic mirror cut-on wavelength: 380 nm (long-pass, LP); barrier filter wavelengths: 420 nm cut-on (long-pass, LP)) and an Andor Clara Interline CCD camera (Oxford Instruments, U.K.). Pictures were taken and processed using ImageJ.[35]

## RESULTS AND DISCUSSION

The working mechanism of the proposed stress self-diagnostic polymeric system is sketched in Figure 1. Its operation is based on the introduction of a tiny amount of fluorescence silent host−guest complexes in the polymer matrix as supramolecular cross-links, which break apart upon mechanical stress in the strained zone leading to localized fluorescence emission.

Since host−guest interactions are considerably weaker than covalent bonds, the disconnection of the supramolecular cross-links takes place well before the covalent bonds are broken, providing an early signal that the mechanical integrity of the


DOI: 10.1021/acs.chemmater.7b02438
Chem. Mater. XXXX, XXX, XXX−XXX

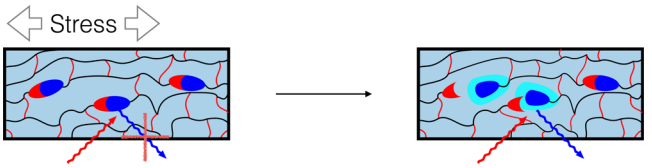


**Figure 1.** Schematic representation of the self-diagnostic polymer working system.

polymer is compromised. Very small quantities of the reporting system are needed; therefore, the physical and mechanical properties of the resulting self-diagnostic polymer are not altered.

**Design and Synthesis of the Host–Guest Reporting Probe and Preparation of the Corresponding PDMS.** The chosen host–guest complex, shown in Figure 2, consists of a tetraphosphonate cavitand as host and an *N*-methylated pyridinium salt as guest. Both the guest and the host are functionalized with terminal double bonds (one in the case of the guest, four in the case of the host), over which the complex is randomly incorporated into the PDMS matrix, thereby adding supramolecular cross-links to the system.

Tetraphosphonate cavitands are versatile molecular receptors capable of binding *N*-methylpyridinium[36] and *N*-methylammonium salts with remarkable selectivity.[37] Tetraphosphonate cavitands form highly stable complexes with *N*-methylpyridinium salts in apolar environments ($K_a$ = 5.8 × $10^6$ $M^{-1}$ in 1,2-dichloroethane)[38] via synergistic cation–dipole interactions between the charged nitrogen and the P=O groups and cation–$\pi$ interactions between the methyl group and the $\pi$-basic cavity.[39] The guest design is inspired by another system reported in the literature,[40] which uses the quenching of a similar guest consisting of an *N*-methylated pyridinium conjugated to a pyrene in combination with calix[*n*]arene-*p*-sulfonates as the artificial acetylcholine detection system.

The incorporation strategy requires the insertion of the reporting system as the preformed complex in the polymer precursors before polymerization, to have complete fluorescence quenching of all guests before mechanical tests. Moreover, the complex must be indefinitely stable in the unstressed polymer. The polymeric matrix compatible with the host–guest complex is a commercial RTV silicone rubber (poly(dimethylsiloxane), PDMS), obtained by the platinum catalyzed reaction of a vinyl PDMS prepolymer with a silicon hydride component (H-PDMS, Figure 3), via formation of ethyl cross-linking bridges between the two.[41]

To incorporate the host–guest complex into the polymer matrix, both the host and the guest are functionalized with $\omega$-alkenyl chains. The terminal double bonds are able to react during the curing of the used PDMS system, inserting the reporting complex randomly into the PDMS matrix. The alkenyl chains are long enough to permit sufficient conformational flexibility to the complex to avoid its mechanical dissociation during the curing of the matrix. The preformed complex is soluble and stable in the PDMS matrix.

The synthesis of the tetraphosphonate cavitand bearing four $\omega$-undecenyl chains is described in the literature.[29,30] Preparation of the guest was performed starting from 4-picoline, which was first alkylated with the double bond terminated linker chain in the benzylic position using *n*-butyllithium. The obtained pyridine was subsequently methylated using iodomethane and the obtained pyridinium salt condensed with 1-pyrenecarboxaldehyde in a Knoevenagel condensation, yielding the desired guest molecule. The host

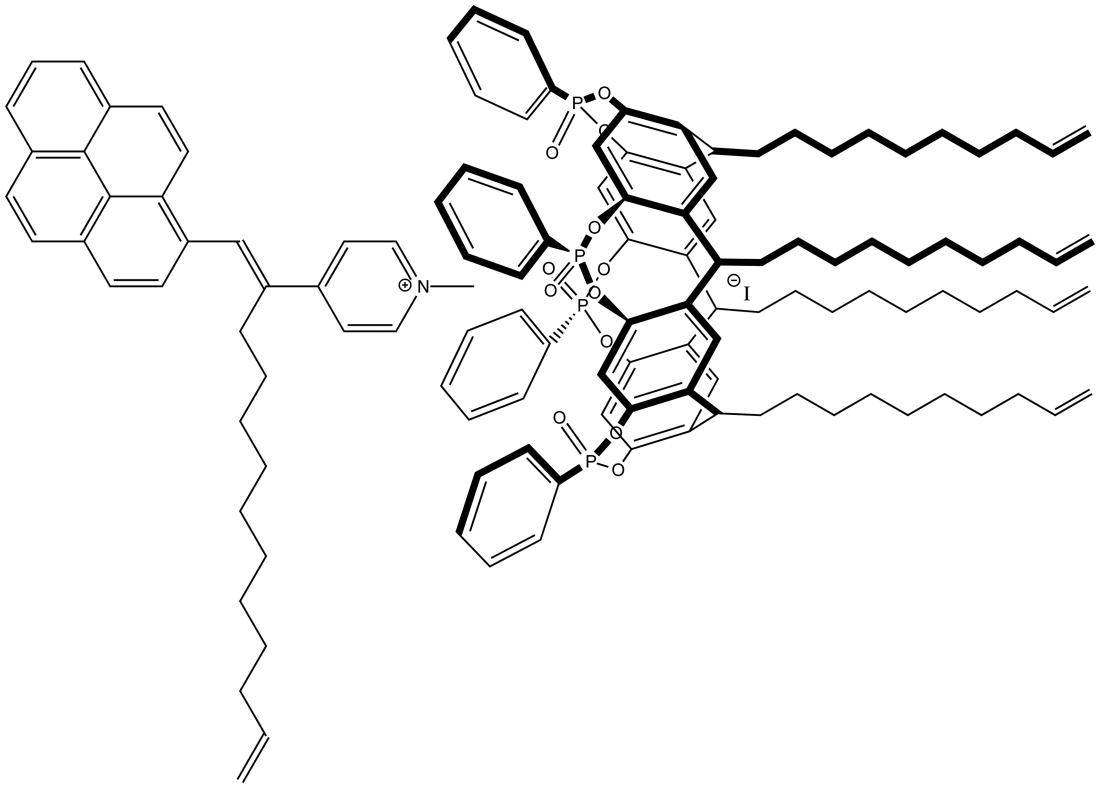


**Figure 2.** Reporting system, consisting of an *N*-methylated pyridinium salt (guest, left) and a tetraphosphonate cavitand (host, right), held together by specific host–guest interactions.



DOI: 10.1021/acs.chemmater.7b02438
*Chem. Mater.* XXXX, XXX, XXX–XXX

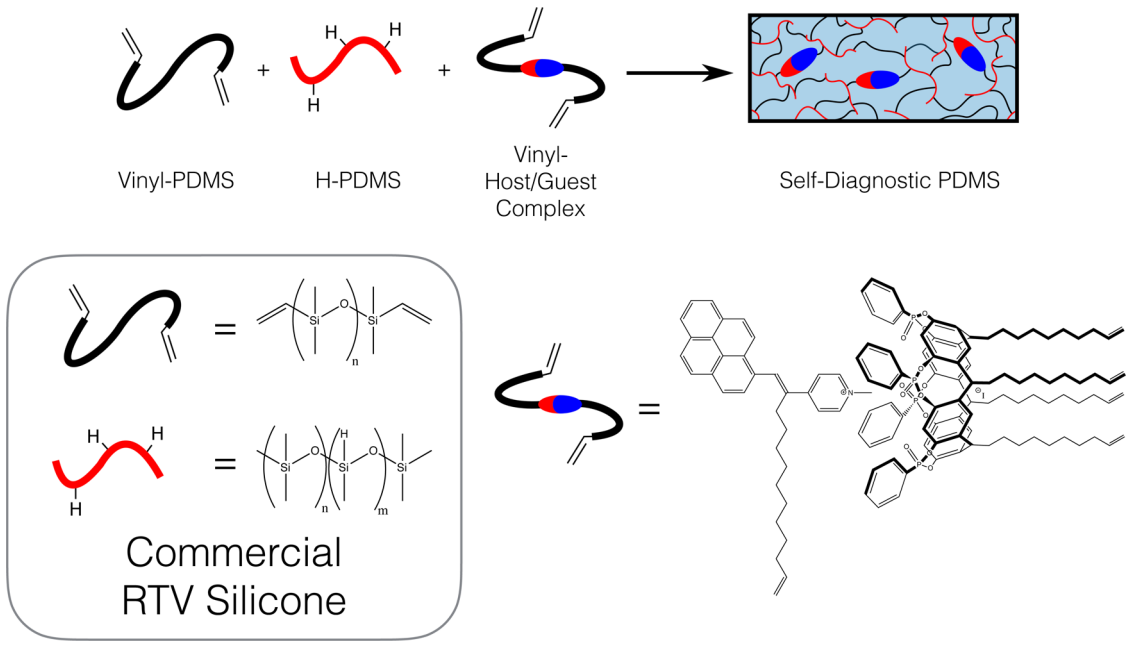


**Figure 3.** Schematic sketch of the self-diagnostic polymer system (top) and the respective chemical structures of the components (bottom).

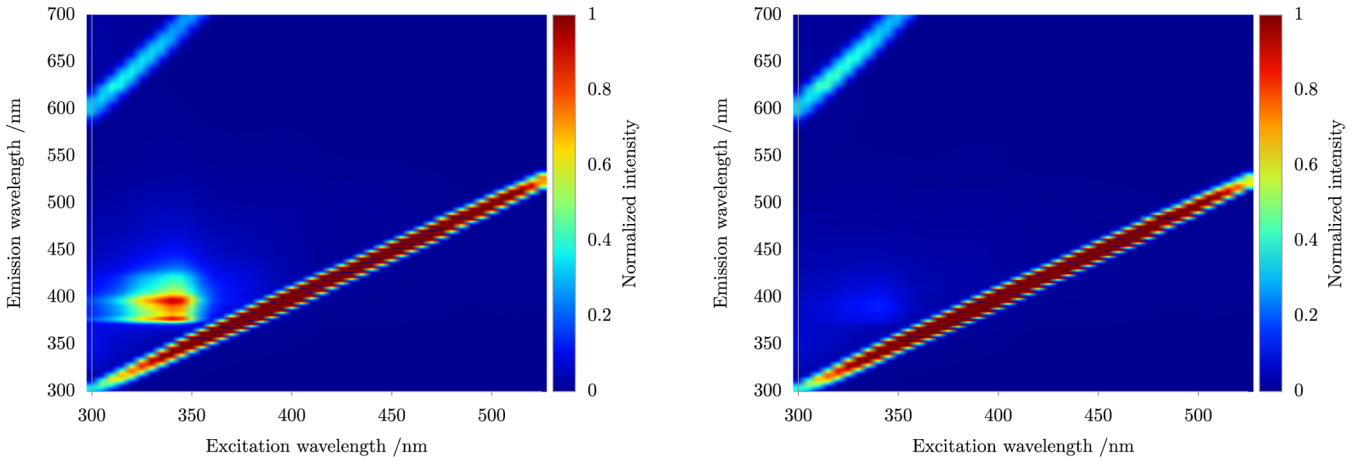


**Figure 4.** Steady-state fluorescence spectra of free guest (left) and the complex in PDMS (right). Both samples contain the guest in a concentration of $b = 10^{-6}$ mol kg$^{-1}$. The two lines are caused by first and second order Rayleigh scattering.

and the guest are then mixed together in dichloromethane (DCM) solution in a 2:1 ratio to form the desired complex. This solution is added to the vinyl−PDMS component, and the residual DCM is removed by heating, giving a homogeneous mixture. Then the H-PDMS and the catalyst are added to the mixture, homogenized, and poured into cuvettes for fluorescent measurements or in molds for mechanical tests. The curing is performed directly into cuvettes and molds by heating them in the oven to 40 °C overnight.

**Fluorescence Characterization.** The reporting complex is designed in a way that its dissociation leads to fluorescence emission. The *N*-methylated pyridinium salt itself, consisting of a pyrene conjugated with the pyridinium system, is highly fluorescent in solution as well as in the PDMS polymer matrix (Figure 4 left). Upon complexation, this fluorescence is quenched (Figure 4, right). This provides an easy and very sensitive method of detection for the dissociation of the complex. In solution, complete complexation of the fluorescent guest is ensured using a twofold excess of the host.

The fluorescence of the guest was measured in DCM solution with a concentration of $c(\text{guest}) = 10^{-6}$ M as well as in PDMS matrix with a concentration $b(\text{guest}) = 10^{-6}$ mol kg$^{-1}$, both in the presence and absence of the cavitand host (see Experimental Section and Figures S1 and S2).

As clearly visible in Figure 4, the guest alone shows an intense fluorescence in the PDMS matrix when excited with ultraviolet light of about $\lambda = 345$ nm with maximum emissions at $\lambda = 380$ nm and $\lambda = 400$ nm. In the complexed state, the fluorescence emission is almost completely quenched. Unfunctionalized PDMS as well as PDMS containing only the host show no fluorescence emission in the measured range (see Figure S2).

**Mechanical Testing and Theoretical Analysis.** The proposed complex, uniformly and isotropically distributed in the polymer matrix, can provide information related to the volumetric strain state in the material upon detachment. Thus, when mechanical stress is applied to the system, it is expected


DOI: 10.1021/acs.chemmater.7b02438
Chem. Mater. XXXX, XXX, XXX−XXX

that the complex will be separated before any damage is done to the material.

**Preliminary Tests.** To test the performances of the reporting probe, specimens containing $10^{-6}$ mol kg$^{-1}$ of the host−guest complex were prepared (Figure 5). The tiny

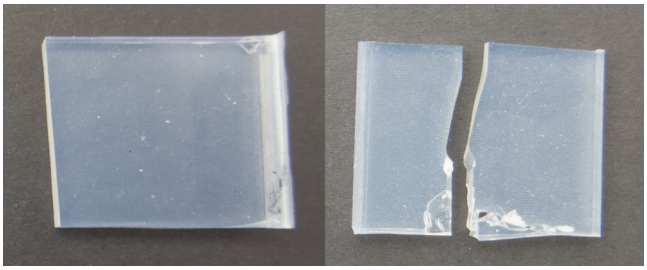

**Figure 5.** PDMS samples before and after breaking.

amount of reporting complex added does not alter the color or transparency of the samples. These specimens were investigated under the fluorescence microscope and subsequently first stretched and then broken. After every step, the fluorescence of each sample was reassessed. As shown in Figure 6, the samples

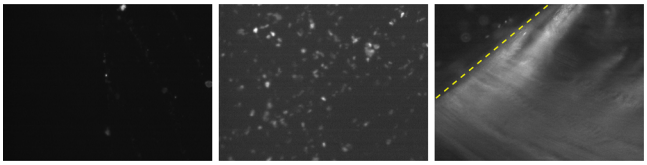

**Figure 6.** Fluorescence images of the sample before stretching (left), after stretching (middle), and after breaking (right). The dashed yellow line indicates the breaking edge.

exhibit no fluorescence in the pristine state (left). However, after stretching, clearly detectable fluorescence features appear (middle), which were even more prominent after breaking the sample and the most intense along the breaking edge (right).

Interestingly, most of the fluorescence is not observed at the fracture edge but in the nearby stressed region. On the basis of those findings, it was decided to investigate the fluorescence emission both theoretically and experimentally.

**Mechanical Characterization.** PDMS specimens, with and without self-diagnostic complexes, have been characterized (Table 1). Because of the chosen geometry of the specimen (Figure 7) and the test procedure, the crack grows in a stable fashion along the middle cross-section of the beam triggered by the initial indentation. The mechanical parameters of the various specimens are almost identical, proving that the addition of the host−guest complex to the matrix does not alter the micromechanical structure of the material. In Table 1 the geometrical and mechanical characteristics of the tested specimens are reported. The addition of the host−guest complex to the matrix does not modify the elastic modulus and the Poisson's ratio of the polymer, which are the two main mechanical characteristics of material. These are the values, together with the material's strength, that must fulfill the design requirements in real applications in order to guarantee the desired mechanical response to external actions.

For sake of completeness, in Table 1 the geometrical parameters (length, width $W$, initial crack depth $a_0$, thickness $t$, and curvature radius $\rho$ at the notch tip) characterizing the precracked beam specimen are also reported (dimensions in Figure 7a); moreover, the energy $\mathcal{G}_c$ necessary for the formation of the unit area of fracture and the fracture toughness related parameter, $K_c$, are also given for the tested materials. The three point bending test has been performed on prenotched specimens, like the one shown in Figure 7b, whose geometry is typical for producing a progressive opening crack growth in Mode I.[42] The loading process has been experimentally monitored using Digital Image Correlation (DIC) analysis. This contactless technique enables the kinematics of the deformation of the material to be measured, without interfering with the specimens.

**Finite Element Analysis.** An accurate finite element (FE) analysis of the specimen has been performed by adopting material elasticity and geometrical nonlinearity. The material behavior being roughly linear elastic up to the first crack growth, a mechanically linear analysis provides the stress and strain values close to the crack tip.

The experimental load versus displacement curve is illustrated in Figure 8a. The evolution of the strained zone extension ahead of the crack tip during the loading process obtained by the FE analysis is shown Figure 8b−d. The numerical results, reporting the horizontal Green−Lagrange strain component $E_{xx}$, refer to the instant before the beginning of the crack growth for $\delta$ = 12 mm, indicated by the arrow in Figure 8a. The corresponding experimental strain map obtained through the DIC analysis is shown in Figure 8e. The dashed lines indicate the profile of the specimen and of the mechanical part used to impose the downward displacement to the upper midspan point of the specimen. The indicated square plates are placed laterally to specimen in order to prevent any possible out-of-plane displacement, i.e., to avoid displacements in the $z$-direction. The correspondence between the experimental and the numerical strain values is satisfactory. These results indicate the region of maximum strain in the specimens during the whole load history, defining spatial region and loading conditions to expect the self-diagnostic fluorescence emission.

**Self-Diagnostic Fluorescence Emission.** In Figure 9 the fluorescence measurements and the relative color map intensity are shown for the blank specimen 1a (see Table 1) in the area around the initial crack tip after the crack started to grow, while in Figure 10 the fluorescence pictures and their color maps are shown for the specimen 1b (the self-diagnostic specimen 1c showed similar results). The small fluorescence spots outside the strained region appearing in Figure 9 are not strain-related fluorescence but are due to dust or small inclusions embedded

**Table 1. Geometrical and Mechanical Characteristics of the Tested Specimens**[a]

| spec. no. | $L$, mm | $W$, mm | $a_0$, mm | $t$, mm | $\rho$, $\mu$m | self-diagnostic | $E$, MPa | $\nu$ | $g_c$, m/N | $K_c$, (MPa $\sqrt{\text{m}}$) |
|---|---|---|---|---|---|---|---|---|---|---|
| 1a | 102 | 25 | 5 | 6 | 150 | no | 0.99 | 0.43 | 111 | 16.2 |
| 1b | 102 | 25 | 5 | 6 | 150 | yes | 0.98 | 0.43 | 108 | 16.2 |
| 1c | 102 | 25 | 5 | 6 | 150 | yes | 1.01 | 0.43 | 110 | 16.2 |

[a] $E$, elastic modulus; $\nu$, Poisson's coefficient; $\mathcal{G}_c$, fracture energy; $K_c$, fracture toughness.



DOI: 10.1021/acs.chemmater.7b02438
Chem. Mater. XXXX, XXX, XXX−XXX

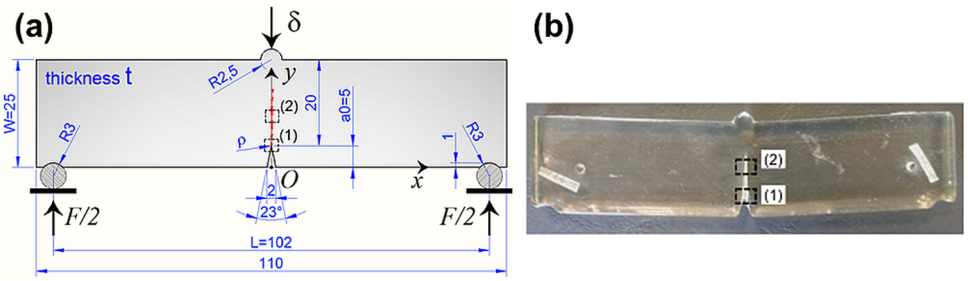


**Figure 7.** (a) Dimensions of the samples used for three-point bending mechanical stress tests (all lengths are given in millimeters). (b) Side view of the specimen after the propagation of the initial crack (after test finish). Locations (1) and (2) where the fluorescence picture have been taken are shown.

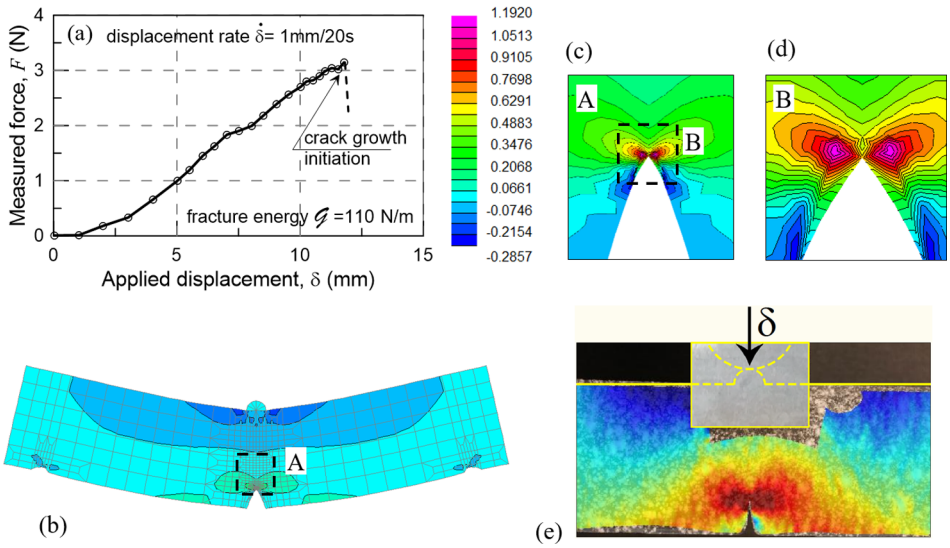


**Figure 8.** Experimental load−displacement curve for the specimen 1b (a). Map of the strain $E_{xx}$ in the deformed beam obtained through the FE analysis (b), related details (c, d), and experimental DIC analysis results (e) of the crack tip region for an applied downward displacement $\delta$ = 12 mm (the Green−Lagrange deformation is displayed in the initial undeformed specimen configuration).

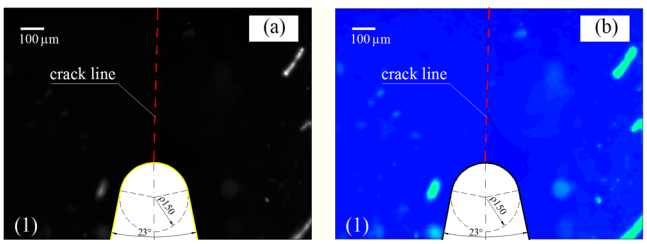


**Figure 9.** (a) Fluorescence image of the crack tip region (1) (see Figures 7a and 10) for the blank specimen 1a. Color map and related normalized intensity scale of the measured fluorescence in the same region (b).

in the material that provide a false brightness in the pictures taken under UV light.

Both the initial notch tip region (1) (Figure 10c,d) and the area along the crack path (2) (Figure 10a,b) have been considered; it can be clearly noted that the fluorescence appears in highly stretched regions. In particular, the stretched area around the initial crack tip shows the highest fluorescence evidence, due to the localized strain arising before the crack growth. This is in accordance to the numerical model and DIC analysis shown in a previous section.

The highest strained region (located at the crack tip) has a very small size compared to the crack, and therefore only a tiny

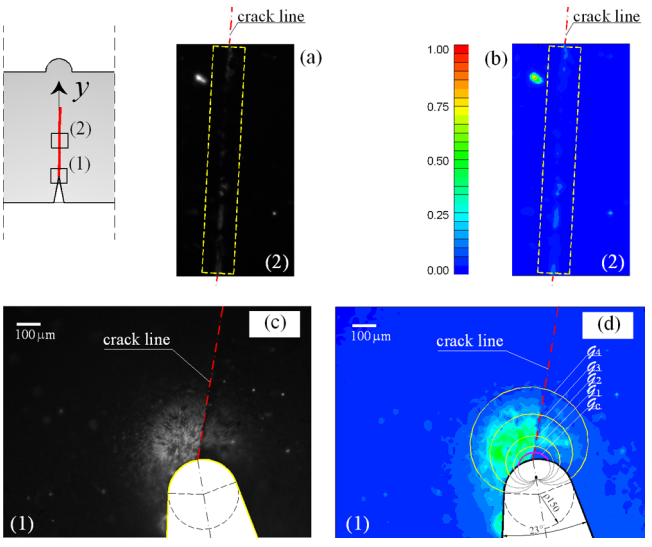


**Figure 10.** (a) Fluorescence images (a, c) and corresponding normalized fluorescence color maps (b, d) of the crack tip region (1) and along the crack growth path (2). In part d the iso-hydrostatic tensile strain curves, obtained by FE analysis, are also plotted: they correspond to the energy values $\mathcal{G}_c$ = 110 N/m (critical energy for material failure) and $\mathcal{G}_1$ = 83 N/m, $\mathcal{G}_2$ = 55 N/m, $\mathcal{G}_3$ = 27 N/m, and $\mathcal{G}_4$ = 11 N/m.



DOI: 10.1021/acs.chemmater.7b02438
Chem. Mater. XXXX, XXX, XXX−XXX

narrow trace of the propagating straight defect can be appreciated in Figure 10a,b.

A proper strain-related quantity needs to be assumed to correlate the fluorescence regions of the stretched specimen to the mechanical deformation. As explained in the Supporting Information, a damage-related parameter can be defined according to the so-called cavitation criterion[27,43] that considers as the primary cause of damage the tensile hydrostatic stress exceeding a certain critical value. The hydrostatic strain represents the mean value, calculated over the normal strains acting in all directions, in a given point of the material. Since the host−guest complex is isotropically oriented inside the polymeric matrix, the number of separated hosts and guests is proportional to the mean strain. It is therefore reasonable to assume that the observed fluorescence intensity provides a measure of the mean strain value.

In Figure 10d the iso-hydrostatic strain curves are displayed (see yellow lines) for different values of the energy ($\mathcal{G}_c > \mathcal{G}_1 > \mathcal{G}_2 > \mathcal{G}_3 > \mathcal{G}_4$, see Supporting Information); in particular the smallest region identified by the pink curve corresponds to the critical energy $\mathcal{G}_c$ (see Table 1) that identifies the damaged region of the material produced by the applied mechanical stress. Outside the curve corresponding to the critical energy $\mathcal{G}_c$, the material is still elastic and recovers completely its initial free-strain state after unloading. However, the cavitand-based sensing system provides a clear trace of the strains previously occurred in the material. It is worth noting that the fluorescence picture and the corresponding map show a certain asymmetry with respect to the crack axis. This can be explained by considering that the crack does not grow along the symmetry axis of the specimen, so the strain field as a result is asymmetric.

## ■ CONCLUSIONS

In conclusion, we prepared and characterized a self-diagnostic PDMS polymer, exploiting the fluorescence properties of a pyrene conjugated *N*-methylpyridinium salt guest in combination with a tetraphosphonate cavitand host. The polymer exhibits no fluorescence when the intact complex is present but a clear fluorescence emission of the guest when dissociated from the host. In this way, it is possible to detect regions of high volumetric strain intensity. The fluorescence maps obtained from a mechanically tested, cracked sample compared with the strain results from numerical analysis and DIC measurements showed a good correlation. We therefore believe that the presented system is suitable for the detection of regions of high volumetric strain in soft polymeric matrices and thus can be used to predict the failure of such materials, increasing their applicability, reliability, and safety level, especially with regard to the in-service maintenance planning. Further, it can be relevant to observe that such a self-sensing strain system can be easily applicable to any structural element by simply coating it with a thin film of the polymer charged with the host−guest cavitand system. If the base material and the coating one adhere perfectly under the application of the mechanical loading, the self-diagnostic layer provides a direct and simple way of quantitatively detecting the strain values in the element underneath.

## ■ ASSOCIATED CONTENT

### Supporting Information

The Supporting Information is available free of charge on the ACS Publications website at DOI: 10.1021/acs.chemmater.7b02438.

Fluorescence characterizations and quantitative modeling (PDF)

## ■ AUTHOR INFORMATION


### Corresponding Authors

*(R.B.) E-mail: roberto.brighenti@unipr.it.

*(E.D.) E-mail: enrico.dalcanale@unipr.it.

### ORCID

Enrico Dalcanale: 0000-0001-6964-788X


### Author Contributions

All authors have given approval to the final version of the manuscript.


### Funding

This work is supported by the Hierarchical Self Assembly of Polymeric Soft Systems (SASSYPOL-ITN) Marie Skłodowska Curie network, funded through the European Union Seventh Framework Programme (FP7-PEOPLE-2013-ITN) under Grant Agreement No. 607602.


### Notes

The authors declare no competing financial interest.

## ■ ACKNOWLEDGMENTS


We thank Davide Orsi for assistance with the fluorescence microscope.


## ■ ABBREVIATIONS

DCM, dichloromethane; DIC, digital image correlation; EtOAc, ethyl acetate; FE, finite element; Hex, hexane; PDMS, poly(dimethylsiloxane); SWCNT, single-walled carbon nanotube; THF, tetrahydrofuran; UV, ultraviolet

## ■ REFERENCES


(1) Clough, J. M.; Balan, A.; Sijbesma, R. P. Mechanochemical Reactions Reporting and Repairing Bond Scission in Polymers. *Top. Curr. Chem.* **2015**, *369*, 209−238.

(2) Black, A. L.; Lenhardt, J. M.; Craig, S. L. From molecular mechanochemistry to stress-responsive materials. *J. Mater. Chem.* **2011**, *21*, 1655−1663.

(3) Li, J.; Nagamani, C.; Moore, J. S. Polymer Mechanochemistry: From Destructive to Productive. *Acc. Chem. Res.* **2015**, *48*, 2181−2190.

(4) Pucci, A.; Bizzarri, R.; Ruggeri, G. Polymer composites with smart optical properties. *Soft Matter* **2011**, *7*, 3689−3700.

(5) Ciardelli, F.; Ruggeri, G.; Pucci, A. Dye-containing polymers: methods for preparation of mechanochromic materials. *Chem. Soc. Rev.* **2013**, *42*, 857−870.

(6) Lee, C. K.; Davis, D. A.; White, S. R.; Moore, J. S.; Sottos, N. R.; Braun, P. V. Force-Induced Redistribution of a Chemical Equilibrium. *J. Am. Chem. Soc.* **2010**, *132*, 16107−16111.

(7) Marelli, B.; Patel, N.; Duggan, T.; Perotto, G.; Shirman, E.; Li, C.; Kaplan, D. L.; Omenetto, F. G. Programming function into mechanical forms by directed assembly of silk bulk materials. *Proc. Natl. Acad. Sci. U. S. A.* **2017**, *114*, 451−456.

(8) O'Bryan, G.; Wong, B. M.; McElhanon, J. R. Stress Sensing in Polycaprolactone Films via an Embedded Photochromic Compound. *ACS Appl. Mater. Interfaces* **2010**, *2*, 1594−1600.

(9) Davis, D. A.; Hamilton, A.; Yang, J.; Cremar, L. D.; Van Gough, D.; Potisek, S. L.; Ong, M. T.; Braun, P. V.; Martínez, T. J.; White, S. R.; Moore, J. S.; Sottos, N. R. Force-induced activation of covalent




DOI: 10.1021/acs.chemmater.7b02438
*Chem. Mater.* XXXX, XXX, XXX−XXX

bonds in mechanoresponsive polymeric materials. *Nature* **2009**, *459*, 68−72.
(10) Klajn, R. Spiropyran-based dynamic materials. *Chem. Soc. Rev.* **2014**, *43*, 148−184.
(11) Chen, Y.; Spiering, A. J. H.; Karthikeyan, S.; Peters, G. W. M.; Meijer, E. W.; Sijbesma, R. P. Mechanically induced chemiluminescence from polymers incorporating a 1,2-dioxetane unit in the main chain. *Nat. Chem.* **2012**, *4*, 559−562.
(12) Ducrot, E.; Chen, Y.; Bulters, M.; Sijbesma, R. P.; Creton, C. Toughening Elastomers with Sacrificial Bonds and Watching Them Break. *Science* **2014**, *344*, 186−189.
(13) Clough, J. M.; Balan, A.; van Daal, T. L. J.; Sijbesma, R. P. Probing Force with Mechanobase-Induced Chemiluminescence. *Angew. Chem., Int. Ed.* **2016**, *55*, 1445−1449.
(14) Chen, Y.; Sijbesma, R. P. Dioxetanes as Mechanoluminescent Probes in Thermoplastic Elastomers. *Macromolecules* **2014**, *47*, 3797−3805.
(15) Robb, M. J.; Li, W.; Gergely, R. C. R.; Matthews, C. C.; White, S. R.; Sottos, N. R.; Moore, J. S. A Robust Damage-Reporting Strategy for Polymeric Materials Enabled by Aggregation-Induced Emission. *ACS Cent. Sci.* **2016**, *2*, 598−603.
(16) Rossi, N. A. A.; Duplock, E. J.; Meegan, J.; Roberts, D. R. T.; Murphy, J. J.; Patel, M.; Holder, S. J. Synthesis and characterization of pyrene-labelled polydimethylsiloxane networks: towards the in situ detection of strain in silicone elastomers. *J. Mater. Chem.* **2009**, *19*, 7674−7686.
(17) Yang, L.; Han, J. Electronic Structure of Deformed Carbon Nanotubes. *Phys. Rev. Lett.* **2000**, *85*, 154−157.
(18) Leeuw, T. K.; Tsyboulski, D. A.; Nikolaev, P. N.; Bachilo, S. M. S. M.; Arepalli, S.; Weisman, R. B. Strain Measurements on Individual Single-Walled Carbon Nanotubes in a Polymer Host: Structure-Dependent Spectral Shifts and Load Transfer. *Nano Lett.* **2008**, *8*, 826−831.
(19) Zeng, S.; Zhang, D.; Huang, W.; Wang, Z.; Freire, S. G.; Yu, X.; Smith, A. T.; Huang, E. Y.; Nguon, H.; Sun, L. Bio-inspired sensitive and reversible mechanochromisms via strain-dependent cracks and folds. *Nat. Commun.* **2016**, *7*, 11802.
(20) Zhang, X.; Chi, Z.; Zhang, Y.; Xu, J.; Liu, S. Recent advances in mechanochromic luminescent metal complexes. *J. Mater. Chem. C* **2013**, *1*, 3376−3390.
(21) Xu, J.; Chi, Z. *Mechanochromic Fluorescent Materials*; Royal Society of Chemistry: Cambridge, U.K., 2014.
(22) Gossweiler, G. R.; Hewage, G. B.; Soriano, G.; Wang, Q.; Welshofer, G. W.; Zhao, X.; Craig, S. L. Mechanochemical Activation of Covalent Bonds in Polymers with Full and Repeatable Macroscopic Shape Recovery. *ACS Macro Lett.* **2014**, *3*, 216−219.
(23) Clough, J. M.; Creton, C.; Craig, S. L.; Sijbesma, R. P. Covalent Bond Scission in the Mullins Effect of a Filled Elastomer: Real-Time Visualization with Mechanoluminescence. *Adv. Funct. Mater.* **2016**, *26*, 9063−9074.
(24) Botsis, J.; Humbert, L.; Colpo, F.; Giaccari, P. Embedded fiber Bragg grating sensor for internal strain measurements in polymeric materials. *Opt. Lasers Eng.* **2005**, *43*, 491−510.
(25) Liehr, S.; Lenke, P.; Wendt, M.; Krebber, K.; Seeger, M.; Thiele, E.; Metschies, H.; Gebreselassie, B.; Munich, J. C. Polymer Optical Fiber Sensors for Distributed Strain Measurement and Application in Structural Health Monitoring. *IEEE Sens. J.* **2009**, *9*, 1330−1338.
(26) Boyce, M. C.; Arruda, E. M. Constitutive Models of Rubber Elasticity: A Review. *Rubber Chem. Technol.* **2000**, *73*, 504−523.
(27) Fond, C. Cavitation criterion for rubber materials: A review of void-growth models. *J. Polym. Sci., Part B: Polym. Phys.* **2001**, *39*, 2081−2096.
(28) Rondeau, R. E. Slush Baths. *J. Chem. Eng. Data* **1966**, *11*, 124.
(29) Misztal, K.; Tudisco, C.; Sartori, A.; Malicka, J. M.; Castelli, R.; Condorelli, G. G.; Dalcanale, E. Hierarchical Self-Assembly of Luminescent $Eu^{III}$ Complexes on Silicon. *Eur. J. Inorg. Chem.* **2014**, *2014*, 2687−2694.
(30) Bibal, B.; Tinant, B.; Declercq, J.-P.; Dutasta, J.-P. Preparation and Structure of [ iiii ] Tetraphosphonatocavitands Bearing Long Chain Functionality at the Lower Rim: Metal Picrates Extraction Studies. *Supramol. Chem.* **2003**, *15*, 25−32.
(31) PerkinElmer. *FL WinLab*; 2001.
(32) Williams, T.; Kelley, C. *gnuplot*; 2016.
(33) Blaber, J.; Adair, B.; Antoniou, A. Ncorr: Open-Source 2D Digital Image Correlation Matlab Software. *Exp. Mech.* **2015**, *55*, 1105−1122.
(34) Blaber, J.; Antoniou, A. *DIC Algorithms*.
(35) Schneider, C. A.; Rasband, W. S.; Eliceiri, K. W. NIH Image to ImageJ: 25 years of image analysis. *Nat. Methods* **2012**, *9*, 671−675.
(36) Yebeutchou, R. M.; Tancini, F.; Demitri, N.; Geremia, S.; Mendichi, R.; Dalcanale, E. Host−Guest Driven Self-Assembly of Linear and Star Supramolecular Polymers. *Angew. Chem., Int. Ed.* **2008**, *47*, 4504−4508; *Angew. Chem.* **2008**, *120*, 4580−4584.
(37) Pinalli, R.; Brancatelli, G.; Pedrini, A.; Menozzi, D.; Hernandez, D.; Ballester, P.; Geremia, S.; Dalcanale, E. The Origin of Selectivity in the Complexation of *N*-Methyl Amino Acids by Tetraphosphonate Cavitands. *J. Am. Chem. Soc.* **2016**, *138*, 8569−8580.
(38) Menozzi, D.; Biavardi, E.; Massera, C.; Schmidtchen, F.-P.; Cornia, A.; Dalcanale, E. Thermodynamics of host−guest interactions between methylpyridinium salts and phosphonate cavitands. *Supramol. Chem.* **2010**, *22*, 768−775.
(39) Pinalli, R.; Dalcanale, E. Supramolecular Sensing with Phosphonate Cavitands. *Acc. Chem. Res.* **2013**, *46*, 399−411.
(40) Koh, K. N.; Araki, K.; Ikeda, A.; Otsuka, H.; Shinkai, S. Shinkai, Reinvestigation of Calixarene-Based Artificial-Signaling Acetylcholine Receptors Useful in Neutral Aqueous (Water/Methanol) Solution. S. *J. Am. Chem. Soc.* **1996**, *118*, 755−758.
(41) Moretto, H.-H.; Schulze, M.; Wagner, G. Silicone. *Ullmann's Encyclopedia of Industrial Chemistry*; Wiley-VCH: Weinheim, Germany, 2000.
(42) Kanninen, M. F.; Popelar, C. H. Advanced fracture mechanics. *Oxford Engineering Science series*; Oxford University Press: Oxford, U.K., 1985.
(43) Lin, Y. Y.; Hui, C. Y. Cavity growth from crack-like defects in soft materials. *Int. J. Fract.* **2004**, *126*, 205−221.


DOI: 10.1021/acs.chemmater.7b02438
*Chem. Mater.* XXXX, XXX, XXX−XXX